Journal of Magnetic Resonance **137,** 206–214 (1999)
Article ID jmre.1998.1652, available online at http://www.idealibrary.com on IDEAL®

Unwanted Signal Leakage in Excitation Sculpting with Single Axis Gradients

Alexej Jerschow

Université de Lausanne, Section de Chimie, BCH, CH-1015 Lausanne, Switzerland

Received August 5, 1998; revised October 27, 1998

Excitation sculpting (T-L. Hwang and A. J. Shaka, *J. Magn. Reson. A* 112, 275–279 (1995)) used for solvent suppression and selective excitation in NMR bases its success on the ability to remove baseline and phase errors created by the application of selective rf pulses. This is achieved by the application of two pulsed field gradient (PFG) echoes in sequence. It is essential that the two pairs of PFGs select the coherence transfer steps independently of each other, which is conveniently achieved if they are applied along orthogonal spatial axes. Here, the much more common case where both PFG pairs must be applied along a single axis is investigated. This is shown to lead to complications for certain ratios of PFG strengths. The original theory of excitation sculpting is restated in the spherical basis for convenience. Some of the effects can only be explained by invoking the dipolar demagnetizing field.

Key Words: **excitation sculpting; pulsed field gradients; coherence pathways; dipolar demagnetizing field; solvent suppression.**

INTRODUCTION

Excitation sculpting (*1–3*) is a powerful method for selective excitation and solvent suppression, which has found many applications in particular in the area of biological NMR where experiments must be carried out in H_2O and where clean selective excitation is crucial (*4–10*). It allows one to suppress phase errors and baseline distortions which are caused by the application of a selective pulse. The sequence can be represented schematically by

$$G_1 - R - G_1 - G_2 - R - G_2, \qquad [1]$$

where G_1 and G_2 represent the pulsed field gradients (PFGs), and R represents a selective pulse (or a combination of selective pulses with hard pulses).

The theory (*1*) states that in order that the artifacts be removed effectively the two gradient pairs should be chosen such that they defocus and refocus independently. One way to ensure this is to apply the two gradient pairs along orthogonal directions in space, thus allowing for a completely independent coherence transfer selection process regardless of the gradient ratio G_1/G_2.

However, very often the experiments must be carried out when only a single gradient direction is available, and the ratio G_1/G_2 becomes critical. This case has not yet been investigated in detail although it concerns the vast majority of the applications in the literature (*4–8, 10*).

THEORY

The spherical basis is convenient for this kind of problem since it allows one to analyze the effects of rf pulses separately from those of the PFGs for each possible coherence pathway (*11*). In this way, artifacts are associated with unwanted coherence pathways surviving the two gradient echoes.

As in the original work (*1–3*) we are interested in the transformation of the input vector **m** into the output vector **M,** both of which are given with respect to

$$\begin{aligned} \mathbf{e}_1 &= -2^{-1/2}(\mathbf{x} + i\mathbf{y}) \\ \mathbf{e}_0 &= \mathbf{z} \\ \mathbf{e}_{-1} &= 2^{-1/2}(\mathbf{x} - i\mathbf{y}). \end{aligned} \qquad [2]$$

The single echo will be considered first, schematically represented by $G_1 - R - G_1$. Without providing specific information on the transformation R we may represent it as an arbitrary rotation characterized by the three Euler angles α, β, γ (the convention of Rose (*12*) is used).

$$R_{mm'}(\alpha, \beta, \gamma) = D^1_{m'm}(\alpha, \beta, \gamma) \qquad [3]$$

(R is the transpose of D^1) and the matrix elements are given by

$$R_{mm'} = \exp(-im'\alpha) d^1_{m'm}(\beta) \exp(-im\gamma), \qquad [4]$$

where the $d^1_{m'm}(\beta)$ are the reduced matrix elements of the Wigner rotation matrix of rank 1.

From the definition of the Euler angles (*12*) we see that β

1090-7807/99 $30.00

can be regarded as the actual (on-resonance) flip angle while α and γ are responsible for offset effects and phase errors.

The action of R on the input vector $\mathbf{m}$ is represented as

$$\mathbf{M} = R\mathbf{m} \qquad [5]$$

with

$$R = \begin{pmatrix} \cos^2(\beta/2)\exp(-i(\alpha+\gamma)) & 2^{-1/2}\sin\beta\exp(-i\gamma) & \sin^2(\beta/2)\exp(i(\alpha-\gamma)) \\ -2^{-1/2}\sin\beta\exp(-i\alpha) & \cos\beta & 2^{-1/2}\sin\beta\exp(i\alpha) \\ \sin^2(\beta/2)\exp(-i(\alpha-\gamma)) & -2^{-1/2}\sin\beta\exp(i\gamma) & \cos^2(\beta/2)\exp(i(\alpha+\gamma)) \end{pmatrix} \qquad [6]$$

The ideal case is considered first (i.e., the gradient pairs defocus and refocus independently): One gradient pair leads to refocusing only if the coherence order changes sign through the action of R, i.e.,

$$G_1p_1 + G_1p_2 = 0 \Rightarrow p_1 = -p_2. \qquad [7]$$

We have thus three possibilities,

$$\begin{aligned} &(1)\ (p_1, p_2) = (1, -1) &&\leftrightarrow s = \sin^2(\beta/2)\exp(-i(\alpha-\gamma)) \\ &(2)\ (p_1, p_2) = (0, 0) &&\leftrightarrow s = \cos\beta \\ &(3)\ (p_1, p_2) = (-1, 1) &&\leftrightarrow s = \sin^2(\beta/2)\exp(i(\alpha-\gamma)), \end{aligned} \qquad [8]$$

where s, the signal attenuation, is taken from Eq. [6].

Due to the action of the second gradient pair (which is assumed to be independent from the first one) only inversion of the coherence order p_2 will be allowed. We are left with the three possibilities

$$\begin{aligned} &(1)\ (p_1, p_2, p_3) = (1, -1, 1) &&\leftrightarrow s = \sin^4(\beta/2) \\ &(2)\ (p_1, p, {}_2p_3) = (0, 0, 0) &&\leftrightarrow s = \cos^2\beta \\ &(3)\ (p_1, p_2, p_3) = (-1, 1, -1) &&\leftrightarrow s = \sin^4(\beta/2), \end{aligned} \qquad [9]$$

where the signals are calculated from Eq. [8] by appropriate combinations.

Defining the "probability for flip," $P = (1 - \cos\beta)/2$, we can draw the complete analogy to the original theory (*1*):

$$\mathbf{M} = \begin{pmatrix} P^2 & 0 & 0 \\ 0 & (1-2P)^2 & 0 \\ 0 & 0 & P^2 \end{pmatrix} \cdot \mathbf{m}. \qquad [10]$$

Phase errors and leakage terms are effectively removed by the application of the second echo, and the input vector is merely scaled. This is, in fact, a simple consequence of the symmetry $D^*_{m'm} = (-)^{m'-m} D_{-m',-m}$ (*12*) from which one can verify the validity of the excitation sculpting principle for arbitrary spin systems when the action of R is describable as a pure rotation.

If both gradient pairs are applied along the same axis, however, one cannot analyze each echo separately. We must consider cases in which complete refocusing is only achieved after the second echo; i.e.,

$$G_1(p_1 + p_2) + G_2(p_2 + p_3) = 0. \qquad [11]$$

If we exclude cases where $G_1 = 0$ or $G_2 = 0$, $p_1 + p_2 = 0$ implies $p_2 + p_3 = 0$ (and *vice versa*) and we have again the following possibilities $(p_1, p_2, p_3) = (1, -1, 1)$, $(-1, 1, -1)$, and $(0, 0, 0)$ as in the uncorrelated case (the signal attenuations will be the same as in Eq. [9]). These are, in fact, the desired pathways, which are always selected, regardless of the gradient ratio G_1/G_2.

Certain ratios, however, will allow also other (unwanted)

TABLE 1
Coherence Pathways Selected by Certain Gradient Ratios and Their Signal Attenuation in Terms of Euler Angles

Number	G_1/G_2	p_1	p_2	p_3	Signal s
1	−2/1	0	1	1	$2^{-3/2}e^{-i(\alpha+2\gamma)}\ (1+\cos\beta)\sin\beta$
2		0	−1	−1	$-2^{-3/2}e^{i(\alpha+2\gamma)}\ (1+\cos\beta)\sin\beta$
3	−1/1	1	1	1	$\frac{1}{4}e^{-2i(\alpha+\gamma)}\ (1+\cos\beta)^2$
4		1	0	1	$-\frac{1}{2}e^{-i(\alpha+\gamma)}\sin^2\beta$
5		0	1	0	$-\frac{1}{2}e^{-i(\alpha+\gamma)}\sin^2\beta$
6		0	−1	0	$-\frac{1}{2}e^{i(\alpha+\gamma)}\sin^2\beta$
7		−1	0	−1	$-\frac{1}{2}e^{i(\alpha+\gamma)}\sin^2\beta$
8		−1	−1	−1	$\frac{1}{4}e^{2i(\alpha+\gamma)}(1+\cos\beta)^2$
9	−1/2	1	1	0	$-2^{-3/2}e^{-i(2\alpha+i\gamma)}\ (1+\cos\beta)\sin\beta$
10		−1	−1	0	$2^{-3/2}e^{i(2\alpha+\gamma)}\ (1+\cos\beta)\sin\beta$
11	1/1	1	0	−1	$\frac{1}{2}e^{-i(\alpha-\gamma)}\sin^2\beta$
12		−1	0	1	$\frac{1}{2}e^{i(\alpha-\gamma)}\sin^2\beta$

Note. Pathways corresponding to the ratios 0, ∞, and 0/0 are removed, since they either cannot be selected or correspond to the trivial cases given in the text.

pathways to leak through. These ratios are determined from Eq. [11] as

$$\frac{G_1}{G_2} = -\frac{p_2 + p_3}{p_1 + p_2}, \qquad [12]$$

which is only meaningful for nonsingular and nonzero values. Table 1 summarizes the coherence pathways that are selected by certain gradient ratios. The signal intensities are calculated by use of Eq. [6]. All pathways in Table 1 are attenuated with phase errors with respect to the desired pathways (Eq. [9]). Therefore, the corresponding gradient ratios have to be avoided.

However, it was found in experiments with excitation sculpting used for solvent suppression that also gradient ratios other than the ones shown in Table 1 led to nonideal behavior (Figs. 3–5). Changing the axis of the applied gradients allowed to attribute these leakage effects to the dipolar demagnetizing field (DDF) (*13–16*). The analysis of DDF effects is hampered by the inherent nonlinear behavior of the equations of motion under the DDF (*13*) and coherence pathways cannot be defined in a conventional way. It was shown that they exhibit multiple quantum coherence like behavior in every aspect of conventional NMR (*14*, *15*). A quantum mechanical theory for these effects was proposed (*14*) where DDF effects were explained by intermolecular multiple quantum coherences. It was also found that while quantitative information was more readily derived from the classical theory (a mean-field approach) the quantum theory allowed to use standard NMR concepts such as coherence pathways to analyze pulse sequences. Recent publications suggest that both approaches are equivalent (*17, 18*).

Usually, the analysis of a complicated sequence (by either theory) is reduced to the case of a two-pulse sequence (*14*) or a three pulse sequence with otherwise strong simplifying assumptions (*19, 20*). The application of a soft pulse for a duration comparable in order to the characteristic "dipolar demagnetizing time" (*14*) $\tau_d = 1/\gamma\mu_0 M_0$ (i.e., ca. 120 ms for a neat H_2O sample in a 7 T magnet) leads to more complications and renders the problem essentially intractable and confined to expensive numerical simulations.

In the present article, effects during the soft pulses are neglected (they are short) and leakage effects using gradient ratios other than the ones listed in Table 1 are attributed to coherence pathways with at least one $|p_i| > 1$. Assuming that the strongest artifacts will be caused by coherence pathways with a next higher order coherence (*14*) Table 2 shows the possible gradient ratios which cause their selection (for brevity only detectable signals after the sequence are considered, i.e., $p_3 = -1$). The extraction of quantitative information about expected signal intensities would require extensive computer simulations. Table 2 thus provides an overcomplete set of gradient ratios (to the extent that we may include higher coherence orders if necessary), the actual significance of which has yet to be shown by experiment.

In the first publication describing DDF effects in NMR (*13*) it was shown that these effects scale with $P_2(\cos\theta)$ where θ is the angle the magnetic field gradient makes with the static B_0 field. Thus by conducting experiments with different angles of the applied gradients it is possible to separate dipolar field artifacts from conventional ones. In particular, at the magic angle, $\cos^{-1}(1/\sqrt{3}) = 54.7$ degrees, the dipolar field effects should vanish completely. Similar effects were shown earlier in the context of water suppression (*21*).

TABLE 2
Coherence Pathways Selected by Certain Gradient Ratios for Absolute Coherence Orders Larger than One (in the Case of Dipolar Demagnetizing Field Effects)

Number	G_1/G_2	p_1	p_2
1	−3/1	1	−2
2	−3/2	0	−2
3	−1/1	−1	2
4	−1/1	−1	−2
5	−3/4	−2	−2
6	−2/3	−2	−1
7	−1/2	0	2
8	−1/2	−2	0
9	−1/3	1	2
10	−1/4	2	2
11	1/2	2	0
12	2/1	2	−1

Note. Pathways involving only single and zero quantum coherences are shown in Table 1. Here, for brevity, only the pathways are listed which are detectable in a water suppression sequence applied at the end of a pulse sequence (i.e., $p_3 = -1$) and which do not correspond to $G_1/G_2 = 0, \infty, 0/0$.

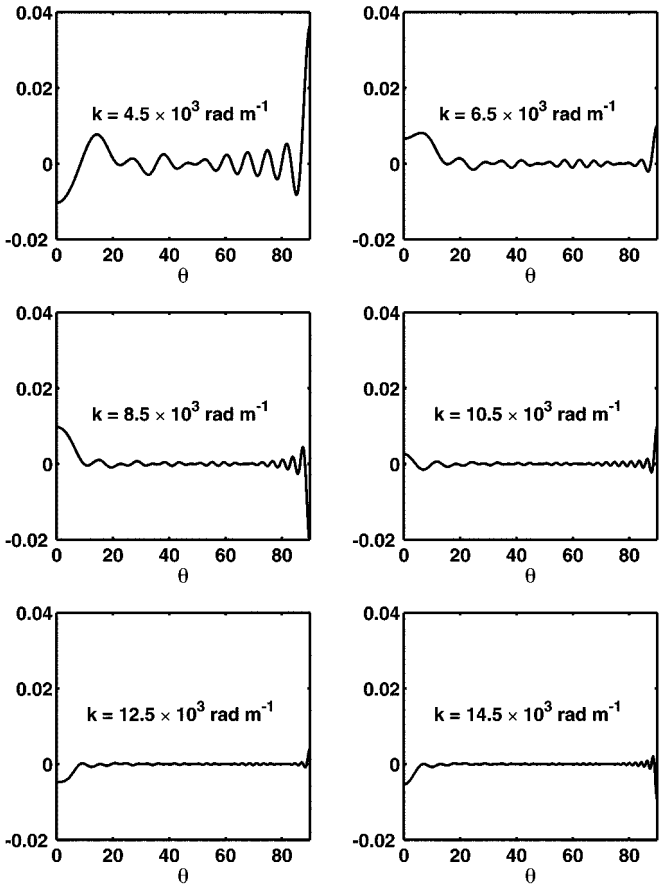

FIG. 1. Attenuation function $s(\theta)$ for coherence pathways according to Eq. [13] depending on the modulation wavelength k and the angle θ of the applied gradient (w.r.t. the B_0 field). The sample is assumed to be a cylinder with $h = 12$ mm, and $r = 2.1$ mm.

If the wavelength of the gradient modulation ($\mathbf{k} = (k_x, k_y, k_z) = \gamma \int \mathbf{G}(t)p(t)dt$) is low (usually $10–10^4$ rad/m) for a particular pathway there can arise effects which may be mistaken for DDF effects through their angular dependence. It was shown recently (*11*) that the gradient attenuation for a cylindrical sample (height h, radius r) is given by

$$s(\theta) = \frac{\sin(k_z h)}{k_z h} \frac{2J_1(k_{xy} r)}{k_{xy} r}, \qquad [13]$$

where $k_{xy} = (k_x^2 + k_y^2)^{1/2}$, and J_1 is the Bessel function of the first kind and first order. Oscillations as a function of the angle θ of the applied gradient are introduced through $k_z = k \cos\theta$, and $k_{xy} = k \sin\theta$ (with $k = |\mathbf{k}|$). Figure 1 shows the function $s(\theta)$ for certain values of k. When k is increased the overall damping becomes stronger but the oscillating features remain. Figure 3 shows experiments where such an angular dependence can be observed. The most important difference to DDF effects is that the latter do not show oscillations. Furthermore, they can be distinguished by the application of stronger gradient pulses where the former are in general attenuated much stronger than the latter (Figs. 4 and 5).

EXPERIMENTAL

The following experiment was conducted,

$$\pi/2 - G_1 - R - G_1 - G_2 - R - G_2 - acqu, \qquad [14]$$

where $R = (\pi_{sel} - \pi)$. $\pi/2$, π are hard rf pulses with the respective nominal flip angles, and π_{sel} is a selective π pulse of duration τ on the water resonance.

All experiments were performed on a Bruker DRX 300 spectrometer (300 MHz proton frequency), equipped with an Acustar gradient amplifier and a multinuclear 5-mm inverse probe (TXI) featuring actively shielded triple axis gradient coils. A 90% H_2O/D_2O sample with 5 mM ubiquitin in an acetate buffer at pH 4.5 at 298 K was used. A gaussian shaped pulse with 1K points, and 1% truncation was chosen for π_{sel}. A single scan of 4K points was acquired in 570 ms. An exponential window function with 2 Hz was applied. To allow sufficient relaxation in between successive experiments a delay of 30 s was included.

Figure 2 shows the spectra acquired for the soft pulse durations $\tau = 3$ and 9 ms with transverse and longitudinal gradients. The quality of the water suppression is excellent in all cases and is the same with the use of orthogonal gradients and longitudinal single-axis gradients. Very high spectral selectivity is achieved for the spectra in Figs. 2c–2f, while J-modulation effects and transverse relaxation attenuation are acceptable.

The experiments shown in Figs. 2b and 2f were conducted for all gradient ratios $G_1/G_2 = m/n$ with $|m|, |n| < 6$. Higher values of m, n were considered practically nonrelevant since very high gradient strengths must be used to adequately distinguish coherence pathways selected, e.g., by the ratios 6/5 and 5/4 while at the same time good water suppression should be provided. To allow a fair comparison between experiments with different gradient ratios the gradient strengths were set such that $|G_1| + |G_2| = G_0 = 0.35$ T/m (=0.49 T/m for the experiment in Fig. 4) and the appropriate settings of G_1 and G_2 (peak amplitude of sine shapes) were calculated by

$$G_2 = G_0/(1 + |m/n|)$$
$$G_1 = G_2 m/n. \qquad [15]$$

The gradient pulse duration was 1.5, 2.2, and 3.5 ms for the experiments of Figs. 3, 4, and 5, respectively (shorter gradient pulses than 1.5 ms resulted in bad water suppression, presumably due to Eddy current effects and gradient area instabilities).

Tilted gradients were performed by combining the z and the

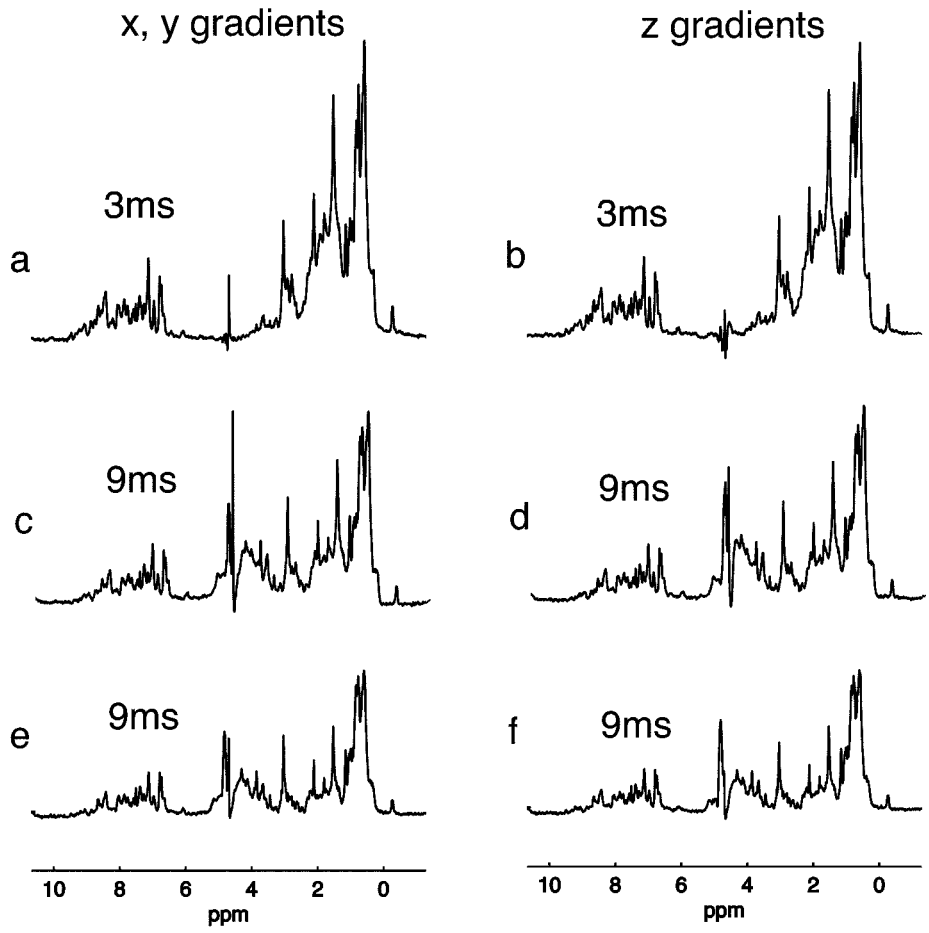

FIG. 2. Excitation sculpting water suppression experiment on a 90% H_2O/D_2O sample with 5 mM ubiquitin. Sine shaped gradients are used. The spectra on the left side are acquired with G_1 along x and G_2 along y with peak strengths of 0.175 T/m each. On the right side z gradients were used with a ratio $G_1/G_2 = 3/1$ ($G_1 = 0.262$ T/m, and $G_2 = 0.088$ T/m). The durations of the gradient pulses are 1.5 ms except for (e) and (f) where they are 3.5 ms. (c–f) show how the selectivity is improved w.r.t. (a–b) due to the longer soft pulse, while J-modulation effects and attenuation due to transverse relaxation are moderate. The apparent improved performance of the single axis gradient experiments (b, d, f) is merely a coincidence.

x gradients with appropriate ratios, the relative strengths of which were calibrated by a simple PFG echo diffusion experiment on water. As a measure to avoid complications from regions with strong gradient nonlinearities the sample was confined to 12 mm in the center of the 17 mm high rf coil by susceptibility-matched plugs as recommended recently (*22*). It was found further that flipping the polarity of both gradients did not change the results for any ratio. All spectra were phased to give in-phase ubiquitin signals.

RESULTS AND DISCUSSION

Figure 3 shows the results of the excitation sculpting experiments with varying flip angles for all gradient ratios. The ratios $-2/1$, $1/1$, and $-1/1$ show severe leakage effects as predicted in Table 1 for $p_3 = -1$ (detection coherence order). It is interesting to note the difference in phase behavior as also indicated in Table 1. The ratio of $-1/1$ corresponds to a case where no effective gradient is experienced in the second evolution period and it shows consequently the most severe artifacts. The ratios $-2/3$, $-3/4$ show an angular dependence with a minimum at the magic angle, which strongly indicates that they are caused by DDF effects (these ratios are featured in Table 2). Other ratios ($-3/2$, $-4/5$, $-3/5$, $-4/3$, $-5/3$, $-5/4$) lead to fairly strong leakage effects of the oscillating type discussed in connection with Eq. [13] and Fig. 1. Weaker effects are observed for $-1/2$, $-1/3$, and $-1/4$. The leakage is mainly due to the coherence pathway (-1, 0, -1). It should be mentioned that these problems are an artifact of the finiteness of the gradient strengths applied. For this reason a second series was performed (Fig. 4) with stronger and longer pulsed field gradients ($G_0 = 0.49$ T/m, 2.2 ms) in order to attenuate

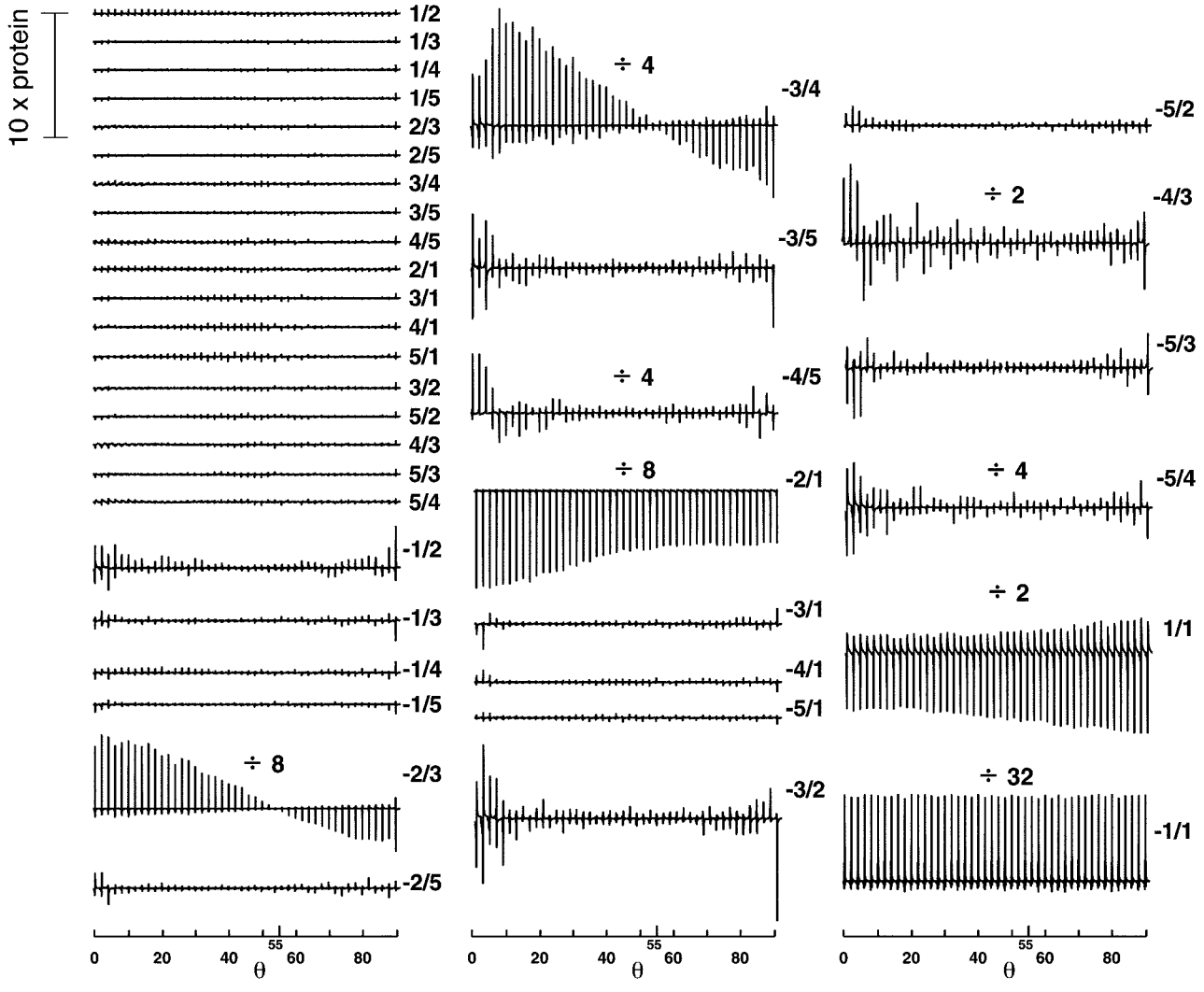

FIG. 3. Excitation sculpting water suppression experiment on a 90% H_2O/D_2O sample with 5 mM ubiquitin. The soft pulse duration is $\tau = 3$ ms, and the gradient pulse duration is 1.5 ms (corresponding to the experiment in Fig. 2b). For each gradient ratio $G_1/G_2 = m/n$ with $|m|, |n| < 6$ the gradient direction was tilted from $\theta = 0$ to 90° in steps of 2. The residual water resonance is shown for all experiments (the region of 4–5 ppm is plotted). The scale indicates the approximate position of the magic angle, 55°. Some spectra were scaled down by the factor indicated to fit in the figure. In the top left corner the tenfold size of the highest protein signal is shown for comparison.

these artifacts. The ratios that lead to DDF effects in the spectra are now unambiguously determined as $-2/3$ and $-3/4$. Even with this setup (long gradient pulses) leakage is still observed from the ratio 1/1 to the ratios 5/4 and 4/5, and also from $-1/1$ to $-5/4$ and $-4/5$.

Figure 5 shows the results of another experimental series conducted with a longer soft pulse ($\tau = 9$ ms) and with gradients of length 3.5 ms and $G_0 = 0.35$ T/m. Here, the same effects are observed. Leakage effects are well suppressed by the long gradients.

Not all of the ratios shown in Table 2 actually have appreciable effects on the spectra (as was discussed in the Theory section) but this may well change at higher fields and with longer evolution delays. It may even be necessary to consider higher coherence orders than two. A strategy to avoid DDF effects can be devised for such cases in the following way.

If the highest possible multiple quantum coherence (involving intermolecular interactions) is p_m and $p_3 = -1$ is fixed (for detection) then the extremal values of the gradient ratios causing refocusing of unwanted pathways are

$$\min\left[\frac{G_1}{G_2}\right] = -p_m - 1$$

$$\max\left[\frac{G_1}{G_2}\right] = p_m. \qquad [16]$$

This follows immediately from Eq. [12] and it can be verified

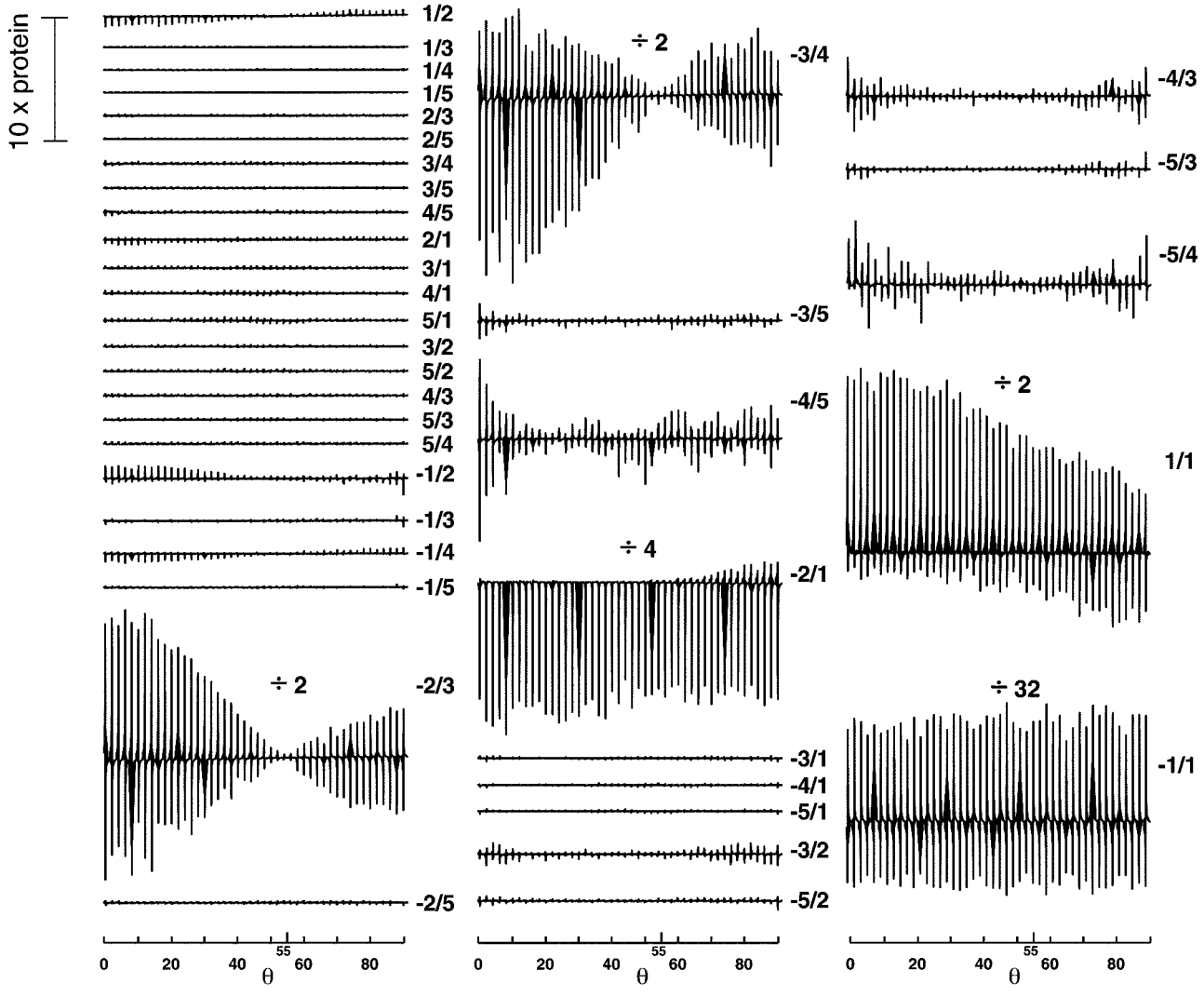

FIG. 4. Same experimental series as in Fig. 3 but with a gradient duration of 2.2 ms, and $G_0 = 0.49$ T/m.

for $p_m = 1$ and 2 in Tables 1 and 2. The value of p_m depends in principle on the field strength, the water concentration, and the duration of the selective pulses and the gradients. As the experiments and Table 2 show, higher coherence orders than two are not necessary to explain the DDF artifacts with the parameters used. Choosing a ratio outside of the range given by Eq. [16] allows one to be always on the safe side.

Radiation damping (*23*) has not yet been considered so far since the bulk water magnetization is usually defocused strongly enough such as not to create coupling with the rf-coil. The only situation in which it could play a significant role is when unmodulated magnetization is rotated into the transverse plane during the soft pulses, or when the magnetization is refocused before the second soft pulse. In both cases the durations of the soft pulses must be comparable to the "radiation damping time" (*23, 24*), which is on the order of 30–60 ms for water at 7 T field strength depending on the quality factor. This time constant is inversely proportional to the macroscopic magnetization and will therefore be much longer if only a fraction of the signal is not modulated.

To refocus the magnetization before the second soft pulse the following condition must be fulfilled:

$$G_1(p_1 + p_2) + G_2 p_2 = 0. \qquad [17]$$

Leaving aside the trivial case $(p_1, p_2) = (0, 0)$ the gradient ratios for this to hold are $G_1/G_2 = -1/2$ for $(p_1, p_2) = \pm(1, 1)$ and $G_1/G_2 = -1$ for $(p_1, p_2) = (0, \pm 1)$. The first ratio did not lead to significant artifacts as is verified in Fig. 5 and the latter is one that must be avoided for other reasons (Table 1). It was thus concluded that radiation damping could be neglected with the parameters used.

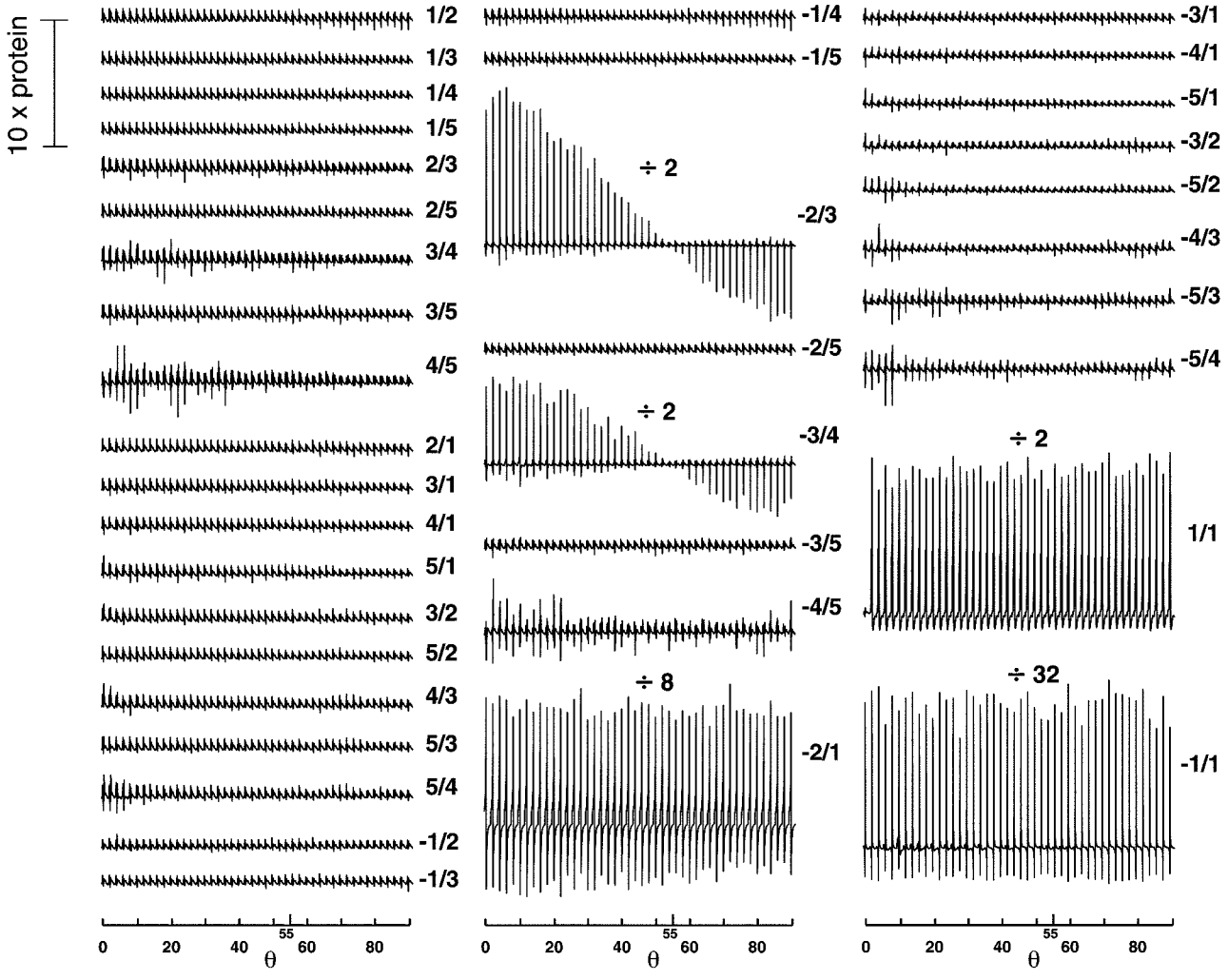

FIG. 5. Same experimental series as in Fig. 3 but with a gradient duration of 3.5 ms and a soft pulse length of $\tau = 9$ ms (corresponding to the experiment in Fig. 2f).

CONCLUSION

It was shown that excitation sculpting using single axis gradients is subject to severe artifacts depending on the gradient ratio G_1/G_2. These effects are well explained by the refocusing (or partial refocusing) of unwanted coherence pathways on the one hand and by dipolar demagnetizing field effects on the other.

Many NMR spectrometers are not equipped with triple axis gradient hardware (where this problem essentially does not arise). In the experiment considered, unwanted signals can be easily avoided by choosing a gradient ratio other than one leading to artifacts of Figs. 3–5, or more safely, outside of the range given by Eq. [16]. Inspection of Figs. 3–5 shows also that more negative ratios are "problematic" than positive ones (essentially all positive ratios except 1/1 are "good"). If the gradients must be applied along one direction in triple axis gradient systems the use of magic angle gradients is in general a good idea.

Multiple excitation sculpting steps require, of course, a more thorough analysis but this can be done easily along the lines outlined in this article (Table 1 for example predicts also complications with a ratio of 1/2 in a pulse sequence where excitation sculpting is applied at the beginning).

ACKNOWLEDGMENTS

The author is grateful for having been able to perform preliminary tests on a 500 MHz spectrometer at the Institut für Chemie, Johannes Kepler Universität Linz, Austria, and for helpful discussions with Norbert Müller, Geoffrey Bodenhausen, Brian Cutting, and Pierre Mutzenhardt. This work was supported by the Fonds National de la Recherche Scientifique (FNRS) and by the Commission pour la Technologie et l'Innovation (CTI) of Switzerland.

REFERENCES

1. T. L. Hwang and A. J. Shaka, Water suppression that works. Excitation sculpting using arbitrary waveforms and pulsed field gradients, *J. Magn. Reson. A* **112,** 275–279 (1995).
2. K. Stott, J. Stonehouse, J. Keeler, T.-L. Hwang, and A. J. Shaka, Excitation sculpting in high-resolution nuclear magnetic resonance spectroscopy: Application to selective NOE experiments, *J. Am. Chem. Soc.* **117,** 4199–4200 (1995).
3. C. Emetarom, T.-L. Hwang, G. Mackin, and A. J. Shaka, Isotope editing of NMR spectra. Excitation sculpting using BIRD pulses, *J. Magn. Reson. A* **115,** 137–140 (1995).
4. K. Stott, J. Keeler, Q. N. Van, and A. J. Shaka, One-dimensional NOE experiments using pulsed field gradients, *J. Magn. Reson.* **125,** 302–324 (1997).
5. K. Stott and J. Keeler, Gradient-enhanced one-dimensional heteronuclear NOE experiment with ^{1}H detection, *Magn. Reson. Chem.* **34,** 554–558 (1996).
6. T. Parella, P. Adell, F. Sánchez-Ferrando, and A. Virgili, Effective multiple-solvent suppression scheme using the excitation sculpting principle, *Magn. Reson. Chem.* **36,** 245–249 (1998).
7. Q. N. Van and A. J. Shaka, Improved cross peak detection in two-dimensional proton NMR spectra using excitation sculpting, *J. Magn. Reson.* **132,** 154–158 (1998).
8. C. Dalvit, Efficient multiple-solvent suppression for the study of the interactions of organic solvents with biomolecules, *J. Biomol. Nucl. Magn. Reson.* **11,** 437–444 (1998).
9. M. Mescher, A. Tannus, M. O'Neil Johnson, and M. Garwood, Solvent suppression using selective echo dephasing, *J. Magn. Reson. A* **123,** 226–229 (1996).
10. G. Mackin and A. J. Shaka, Phase-sensitive two-dimensional HMQC and HMQC–TOCSY spectra obtained using double pulsed-field-gradient spin echoes, *J. Magn. Reson. A* **118,** 247–255 (1996).
11. A. Jerschow and N. Müller, Efficient simulation of coherence transfer pathway selection by phase cycling and pulsed field gradients in NMR, *J. Magn. Reson.* **134,** 17–29 (1998).
12. M. E. Rose, "Elementary Theory of Angular Momentum," Wiley, New York (1966).
13. G. Deville, M. Bernier, and J. M. Delrieux, NMR multiple echoes observed in solid ^{3}He, *Phys. Rev. B* **19,** 5666–5688 (1979).
14. S. Lee, W. Richter, S. Vathyam, and W. S. Warren, Quantum treatment of the effects of dipole–dipole interactions in liquid nuclear magnetic resonance, *J. Chem. Phys.* **105,** 874–900 (1996).
15. M. H. Levitt, Demagnetization field effects in two-dimensional solution NMR, *Concepts Magn. Reson.* **8,** 77–103 (1996).
16. R. Bowtell, R. M. Bowley, and P. Glover, Multiple spin echoes in liquids in a high magnetic field, *J. Magn. Reson.* **88,** 643–651 (1990).
17. W. S. Warren and S. Ahn, The boundary between liquidlike and solidlike behavior in magnetic resonance, *J. Chem. Phys.* **108,** 1313–1325 (1998).
18. J. Jeener, A. Vlassenbroek, and P. Broekaert, Unified derivation of the dipolar field and relaxation terms in the Bloch–Redfield equations of liquid NMR, *J. Chem. Phys.* **103,** 1309–1332 (1995).
19. I. Ardelean, R. Kimmich, S. Stapf, and D. E. Demco, Multiple nonlinear stimulated echoes, *J. Magn. Reson.* **127,** 217–224 (1997).
20. I. Ardelean, S. Stapf, D. E. Demco, and R. Kimmich, The nonlinear stimulated echo, *J. Magn. Reson.* **124,** 506–508 (1997).
21. D. L. Mattiello, W. S. Warren, L. Mueller, and B. T. Farmer II, Minimizing the water resonance in biological NMR: Characterization and suppression of intermolecular dipolar interactions by multiple-axis gradients, *J. Am. Chem. Soc.* **118,** 3253–3261 (1996).
22. A. Jerschow and G. Bodenhausen, Mapping the B_1 field distribution with non-ideal gradients in a high-resolution NMR spectrometer, *J. Magn. Reson.* **137,** 108–115 (1999).
23. A. Vlassenbroek, J. Jeener, and P. Broekaert, Radiation damping in high resolution liquid NMR: A simulation study, *J. Chem. Phys.* **103,** 5886–5897 (1995).
24. X.-A. Mao and C.-H. Ye, Understanding radiation damping in a simple way, *Concepts Magn. Reson.* **9,** 173–187 (1997).